J Mater Sci (2007) 42:7354–7362
DOI 10.1007/s10853-007-1554-5

Particle distribution and interfacial reactions of Al–7%Si–10%B_4C die casting composite

Zhan Zhang · X.-G. Chen · A. Charette

Received: 5 September 2006 / Accepted: 25 January 2007 / Published online: 15 May 2007

Abstract Aluminum–boron carbide particle reinforced composite is an advanced material which can be used in applications such as neutron-shielding components, aircraft, and aerospace structures. In the microstructural characterization of an Al–7%Si–10%B_4C die casting, attention is particularly focused on particle distribution and interface reaction products between B_4C particles and the aluminum matrix. The quantitative analysis results show that, in a cross-section of the cast part, more particles concentrate in the center and fewer particles are present in the wall regions. Moreover, some particle segregation bands have been observed. The mechanisms of the particle migration are proposed to describe the phenomenon. However, the average particle fraction in any cross-section of the cast part is almost the same. A barrier layer consisting of several sublayers was detected on the surface of B_4C particles. Using electron diffraction in selected areas, it is found that these sublayers are composed of Al_3BC crystals, TiB_2 crystals, Si crystals, and coarse stick-shaped TiB_2 particles. In addition, it is observed that Si plays an important role in the formation of a dense barrier layer. The barrier layer can limit B_4C decomposition and improve B_4C stability in the aluminum melt.

Z. Zhang (✉) · A. Charette
Université du Québec à Chicoutimi, Chicoutimi, QC, Canada G7H 2B1
e-mail: zhan_zhang@uqac.ca

X.-G. Chen
Alcan Inc., Arvida Research and Development Centre, Jonquiere, QC, Canada G7S 4K8

Introduction

Al–B_4C metal–matrix composites are being considered as new advanced materials due to their ability to capture neutrons, as well as their light weight, high stiffness, and hardness [1–4]. Generally, processes for the manufacture of aluminum-based metal–matrix composites (MMCs) include: (1) the liquid mixing process, and (2) the powder metallurgy process. The liquid mixing process is an effective method to economically produce large quantities of Al-based metal–matrix composites. This process has been employed to produce most of the commercial Al-based metal–matrix composites such as Al–SiC and Al–Al_2O_3 MMCs [5]. However, since there are strong chemical reactions between B_4C and Al, it would be difficult to use this process to produce Al–B_4C composites if the interfacial reactions cannot be controlled [4–9]. Viala et al. reported that when the Al–B_4C temperature is between 660 and 868°C, the reaction products are Al_3BC and AlB_2 [6]. Currently, a novel liquid mixing process has been developed to commercially produce the composites [1, 2]. In this process, titanium is added into the composite melt to form a barrier layer on the surface of B_4C particulate. This barrier layer can limit the interfacial reactions between the B_4C and the aluminum matrix [2, 9]. Based on thermodynamic calculations and chemical identification, the barrier layer consists of compounds containing titanium [2, 9]. However, the detailed chemistry and phases of the layer have not yet been clearly identified.

High pressure die casting is an economical and effective process to produce net-shaped aluminum castings. In the process, the melt, under a high pressure (30–80 MPa), is injected into the cavity of a die at a high velocity (10–40 m/s) and the solidification of the castings takes place under high pressure. Under some circumstances, a

segregation band defect can be observed in die cast parts. This defect has recently received significant research attention [10–14]. Dahle and Stjohn proposed an explanation of this phenomenon [15]. The theory relates the formation of a segregation band to the mechanical behavior of the partially solidified microstructure when shear stresses develop during the filling of a cast part. The band formation can be summarized as follows. When the slurry, a mixture of melt and externally solidified crystals, is injected into the die cavity, a part of the slurry contacting the die wall solidifies due to the rapid cooling from the die wall. When the flowing slurry passes the solidified layer, a shear stress between the layer and the slurry arises. This shear could result in segregation bands and shear-related defects. In the die cast parts of aluminum–matrix composites, it was observed that the particle distribution was not uniform [16–18]. However, there is very limited public information available concerning the impact of the segregation band on the particle distribution in Al–matrix composite die castings.

Controlling particle distribution in the matrix is very important for composite material application since it greatly impacts the mechanical properties such as tensile strength and elongation of the materials [19]. It is suggested that the particle distribution in the solidification process could be determined by: (1) pushing the particulates by solid/liquid growth interface, (2) trapping by dendrites, (3) particle settling or flotation, (4) particle size, (5) solidification cooling rate, (6) nucleation process and (7) chemical reactions [16–20]. The phenomenon of non-uniform particulate distribution in the matrix often occurs in particle reinforced aluminum composite die castings, and it was reported that plunger velocity and particle size have a great influence [7, 18]. However, despite previous studies, the effect of composite fluid flow on particulate migration and the resulting distribution have yet to be satisfactorily clarified.

In this paper, the investigation of the composite microstructure is focused on quantitative particle distribution analysis and identification of interfacial reaction products to better understand the behavior of particle migration in the die casting process and to identify the components of the barrier layer.

Experimental procedure

To prepare the composite, commercially pure aluminum was first melt in an electric resistance furnace. Prefabricated AA1100-25%B_4C cast billets by Alcan, along with Si, Mg and Ti alloying elements were added into molten aluminum in such proportions that the final composite melt consisted of 10 vol.%B_4C, 7 wt.%Si, 0.5 wt.%Mg, and 2 wt.%Ti. The average B_4C particle size was approximately 23 μm. During the batch operation, the composite melt was held under mechanical stirring to ensure a uniform distribution of B_4C particles in the liquid. The temperature of the melt was maintained at 690–700 °C. A 600-ton Buhler cold chamber die casting machine was used to produce the parts (a box type). The surface of the die was kept at 200 °C when pouring each cast part. An experimental cast part of the composite is shown in Fig. 1a and b.

To examine the microstructure, the cast part was cut along sections A–A and B–B (Fig. 1a). Six samples were selected at different distances from the pouring gate (Fig. 1a). The wall thickness and the distance from the gate at the sampling positions are given in Table 1.

For the quantitative evaluation of particle distribution in the matrix, the particle fraction in each field of view was measured by using an optical image analyzer (CLEMEX JS-2000, PE 4.0) at two hundred times magnification. To ensure a good statistical representation, three zones (I, II, and III) across the wall thickness of a sample were selected (Fig. 2). In each zone, the particle fractions were sequentially measured from the outside wall towards the center and finally to the inside wall. Results of the quantitative measurements were statistically analyzed.

An optical microscope, an electron probe microanalyzer (EPMA, CAMECA SX-100) equipped with a wavelength dispersive spectrometer (WDS) and a transmission electron microscope (TEM, JEM 2100F) were used to identify the

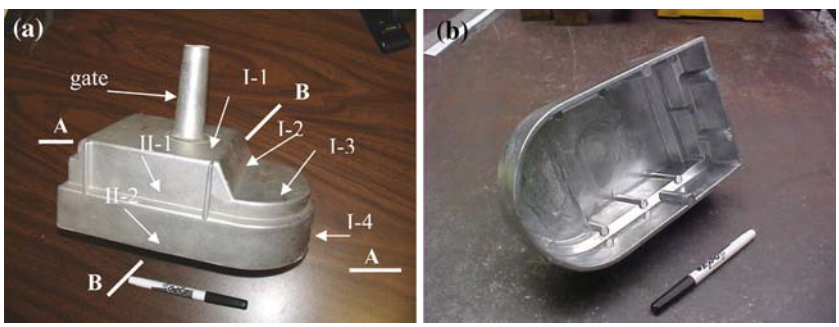

Fig. 1 An experimental cast part and sampling positions: (**a**) outside view, (**b**) inside view

Table 1 Wall thickness and sampling distance from gate

Samples	Wall thickness (mm)	Distance from gate (mm)
I-1	8	15
I-2	6	40
I-3	6.5	90
I-4	4.5	160
II-1	6	60
II-2	4.5	110

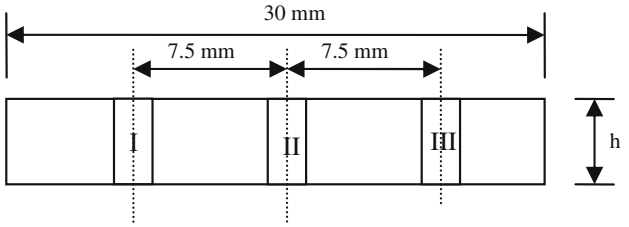

Fig. 2 Sketch of three analysis zones in each sample (h: wall thickness of the part; I, II, and III: analysis zones)

interfacial reaction products between the B_4C particles and the Al matrix.

Results and discussion

Particle distribution

Figure 3 shows a typical B_4C particle distribution in a sample cross-section by means of an optical microscope. Generally, the amount of B_4C particles is less in the regions near the die walls than that in the center. The results of the quantitative evaluation of samples I-1 and I-4, as example, are shown in Fig. 4. In regions near the die walls, there are fewer B_4C particles in the matrix. Towards the center, more B_4C particles are found in the matrix. Sample I-1, for example, has a wall thickness of 8 mm and the region that has fewer particles is approximately 2 mm in width from the wall. The minimum particle fraction in the wall region is approximately 6%. The maximum particle fraction in the center region can reach up to 17%. The same tendency of particle distribution has been confirmed in all samples although the wall thickness in the six samples varies from 4.5 to 8 mm. Hence, the particle distribution in the cross-section is not uniform, i.e., more particles concentrate on the center and fewer particles locate in the near die wall regions.

On the other hand, the average fractions of particles in the cross-sections of the six samples are about the same. Table 2 gives the average particle fraction and standard deviation of all analyzed zones in the six samples. By means of a simple two-sided student's *t*-test at 95% level of significance, the average particle fraction in these samples is not significantly different. It should be noted that the six samples were taken at different distances from the filling gate. Sample I-1 is close to the gate while samples I-4 and II-2 are at the end of the cast part. It is therefore reasonable to believe that the average particle fraction in any cross-section of the cast part would be at the same level.

In addition, there are a few segregation bands existing in the cross-section of the cast parts (Fig. 3). One of the most obvious bands is directly near the outside die wall, where there are only a few particles contained within the band.

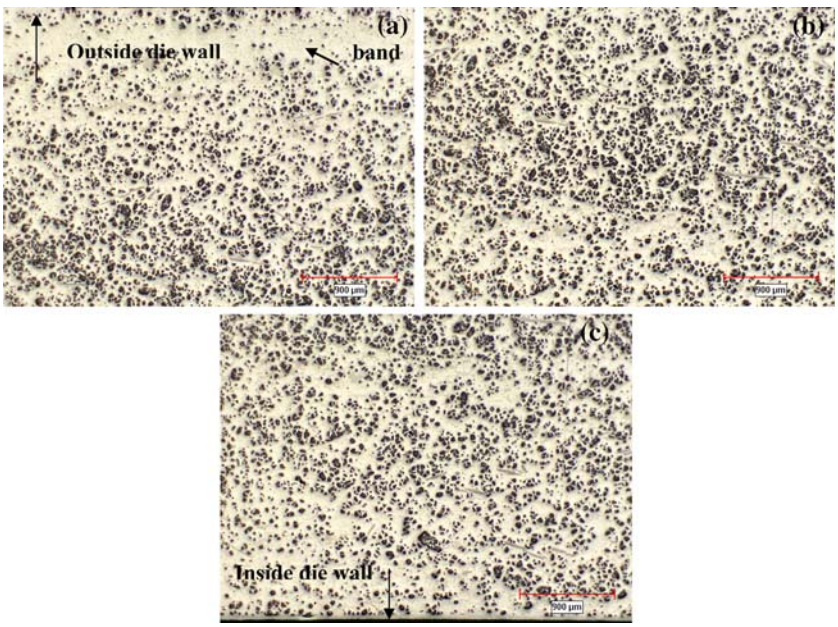

Fig. 3 Typical B_4C particle distribution: regions (**a**) near the outside die wall, (**b**) in the center, (**c**) near the inside die wall

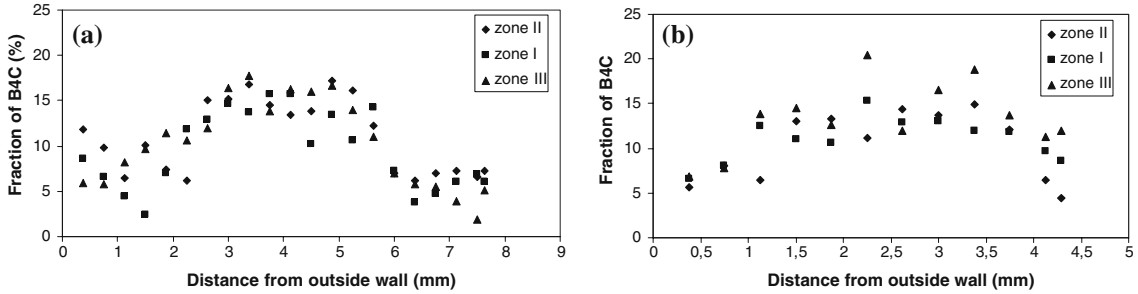

Fig. 4 Particle distribution: (**a**) in sample I-1, (**b**) in sample I-4

Table 2 Particle fraction in the samples

Sample	Analyzing zone	Average fraction in a zone (%)	Standard deviation in a zone (%)	Average fraction in a sample (%)	Standard deviation in a sample (%)
I-1	Zone I	9.37	4.24	10.14	4.37
	Zone II	10.82	4.01		
	Zone III	10.22	4.84		
I-2	Zone I	9.70	4.75	10.14	4.17
	Zone II	10.09	4.57		
	Zone III	10.65	3.23		
I-3	Zone I	12.80	2.75	12.51	3.38
	Zone II	11.80	2.74		
	Zone III	12.92	3.55		
I-4	Zone I	10.99	2.34	11.13	3.06
	Zone II	10.31	3.68		
	Zone III	12.38	3.82		
II-1	Zone I	11.06	3.26	10.75	3.47
	Zone II	11.03	3.03		
	Zone III	10.16	3.96		
II-2	Zone I	10.53	4.1	10.68	3.46
	Zone II	10.48	2.11		
	Zone III	11.02	4.17		

In die casting, the solidification and fluid flow processes may have an impact on the particle distribution. During the early stages of solidification, the solid fraction near the die walls is greater than that in the center, and the size of alpha-Al grains is much less than that in the center due to the cooling from the walls (Fig. 5). These would result in gradually enlarging the melt channels through which particles can be pushed towards the center by the growing primary alpha-Al grains. When the particle movement is impeded by narrow ''channels'', particles are enclosed in grains. Otherwise, particles are further pushed towards the center. As a result, more particles should be located near the center. Actually, it was found that the particles are pushed to the last freezing zone and are enclosed by the growing dendrites in the region near the die wall (Fig. 5a). However, when the size of alpha-Al is larger than that of the particles, the particles can be entrapped by alpha-Al dendrites (Fig. 5b). Moreover, in a particle suspension system, fluid flow influences particle distribution [13, 15, 21]. The particles in the dispersion system move towards the center where shearing is at a minimum [21]. Therefore, the particle migration would be attributed to grain pushing and fluid rheologic behaviors. The two mechanisms of particle movement can be described as shown in Fig. 6.

In addition, when a solidified layer is formed on the die wall and the flowing composite melt passes the layer, the shear force between the solidified layer and the melt flow would result in a segregation band near the outside wall (Fig. 3), in which there are only a few solid particles. The reason for the segregation band formation could be as follows. When the composite melt, a mixture of particles and liquid aluminum, is injected into the die cavity, a part of the melt contacting the die wall will first solidify due to the cooling from the die wall. When the flowing melt passes the solidified layer, a shear stress between the layer

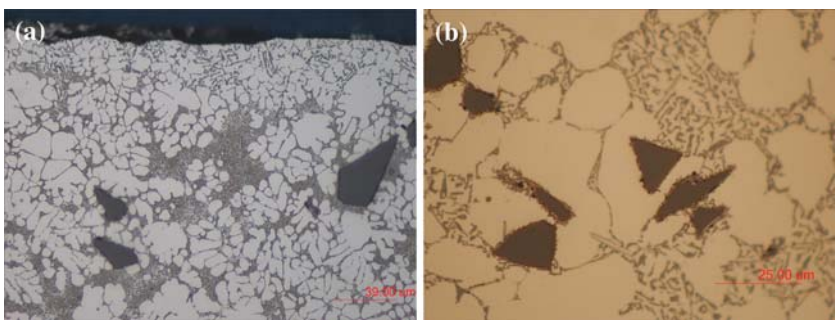

Fig. 5 Al grains and B_4C particles in the microstructure: (**a**) near the die wall, (**b**) in the center

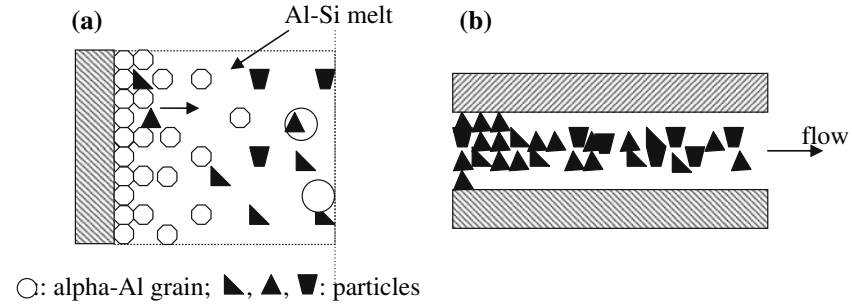

Fig. 6 Sketches of particle movement: (**a**) pushing and enclosing, (**b**) impact from fluid flow

and the melt arises. In order to reduce the shear stress, the liquid concentrates on the surface of the solidified layer as a lubricant. This would result in the formation of the segregation band that contains a few particles. However, the formation of the band is dependent on the existence of the solidified layer. When the solidified layer is removed by the melt at a high speed or the temperature of the die wall is high enough to prevent the formation of the solidified layer, the segregation band would be less obvious.

Interfacial reactions

Since B_4C is not stable in an aluminum melt, the particles may react with the aluminum to form reaction products such as AlB_2 and Al_3BC which deteriorate the fluidity of the melt and certain mechanical properties [1, 2, 9, 19]. As a novel technique, it was found that, by adding higher levels of Ti (approximately 2%) in this Al–7%Si–10%B_4C composite, most B_4C particles become stable in the aluminum matrix. No significant degradation of B_4C was observed.

Figure 7 shows a backscatter electron image and corresponding titanium mapping by using an electron probe microanalyzer. All the B_4C particles still have good shapes and edges indicating that no remarkable decomposition of the particles occurs. A barrier layer containing titanium was detected on the surfaces of all B_4C particles. Since the thickness of the layer is generally less than 1 μm, a transmission electron microscope (TEM) was employed to identify the structure and components of this layer.

The TEM electron images and line scans of the elements are shown in Figs. 8 and 9. The barrier layer can be divided into two locations: location A and location B, based on the

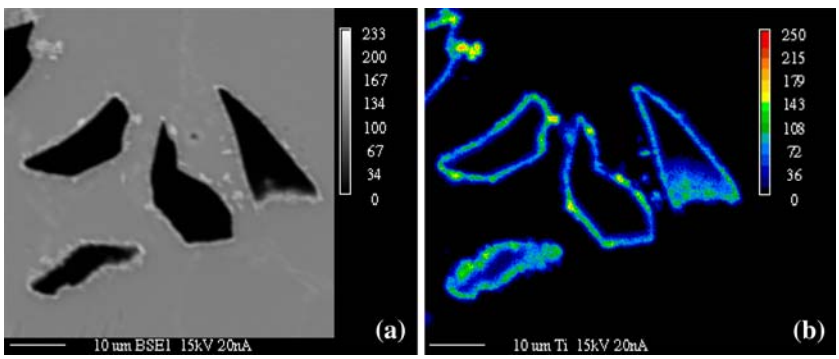

Fig. 7 B_4C interfaces: (**a**) a backscatter electron image, (**b**) titanium mapping

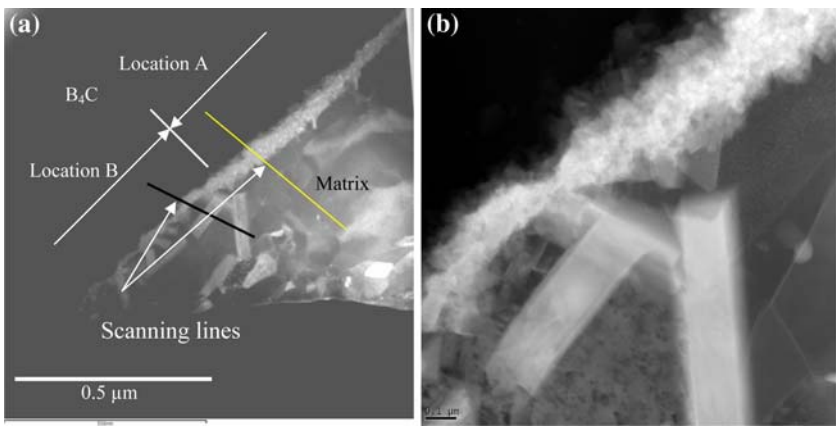

Fig. 8 TEM electron micrographs: (**a**) a dark-field image showing the barrier layer around the B_4C particle, (**b**) an enlarged view

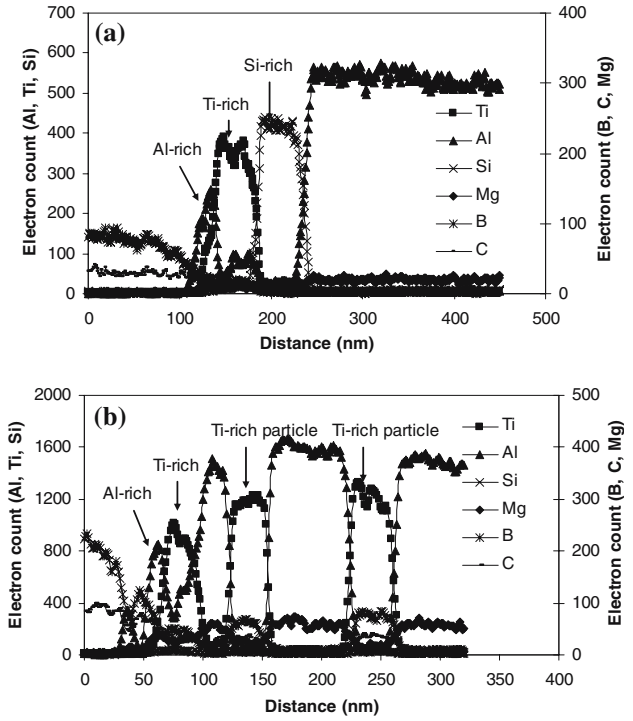

Fig. 9 Element distribution in line scan routes: (**a**) in location A, (**b**) in location B

morphology of the layer. In location A, the layer consists of three sublayers (Figs. 8 and 9a). A tiny aluminum-rich sublayer (approximately 100 nm) was detected close to the surface of B_4C particles. This Al-rich sublayer contains boron, carbon, and traces of magnesium. The second sublayer is a Ti-rich lamella containing B, and traces of Al, C, Mg, and Si. This sublayer is composed of many fine crystals on a nanometer scale. The last sublayer is Si-rich and contains traces of magnesium and aluminum. However, the Si-rich sublayer is not continuous around the surfaces of the B_4C particles.

TEM electron diffraction patterns obtained in selected areas proved to be effective for identifying the compounds and phases in the sublayers. As an example, the transmission electron micrographs and the diffraction patterns in the Al-rich and Ti-rich sublayers in location A are shown in Figs. 10 and 11. By comparison of the measured diffraction patterns with those from standard powder diffraction files [22], the compounds in Al-rich sublayer are identified as fine crystals of Al_3BC. In the Ti-rich sublayer, it is confirmed that this layer is composed of fine TiB_2 crystals. Moreover, in Si-rich sublayer, the crystals in the sublayer have the same structure as that of Si crystals (Fig. 12) [23]. The Si crystals should come from Al–Si eutectics.

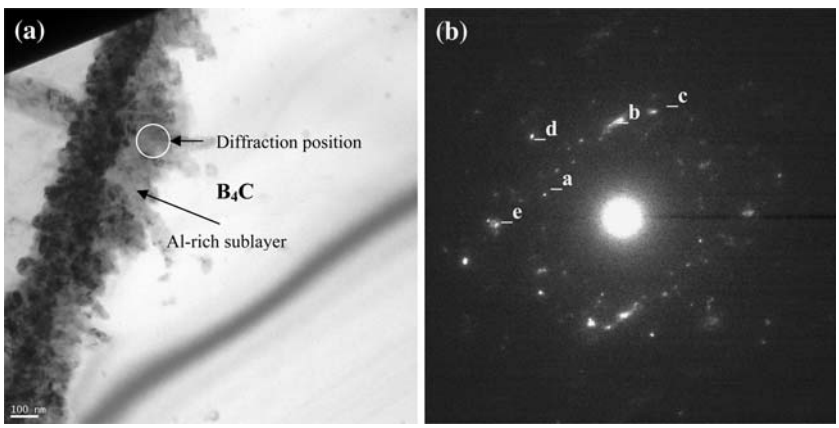

Fig. 10 TEM observations of Al-rich sublayer (Al_3BC) close to the B_4C particle: (**a**) a bright-field image showing the sublayer and the position of electron diffraction, (**b**) corresponding selected area diffraction ring patterns from polycrystalline Al_3BC: a, (004); b, (103); c, (104); d, (006); e, (105)

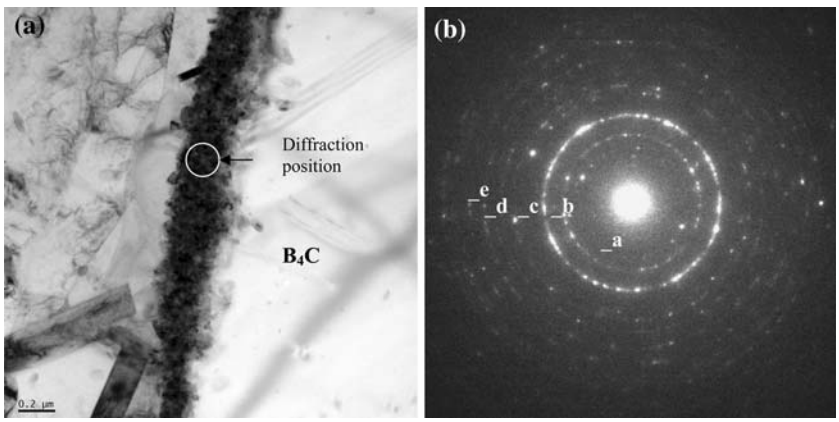

Fig. 11 TEM observations of Ti-rich sublayer (TiB_2): (**a**) a bright-field image showing the sublayer (dark) and the diffraction position, (**b**) corresponding selected area electron diffraction ring pattern from polycrystalline TiB_2: a, (100); b, (101); c, (002); d, (110); e, (102)

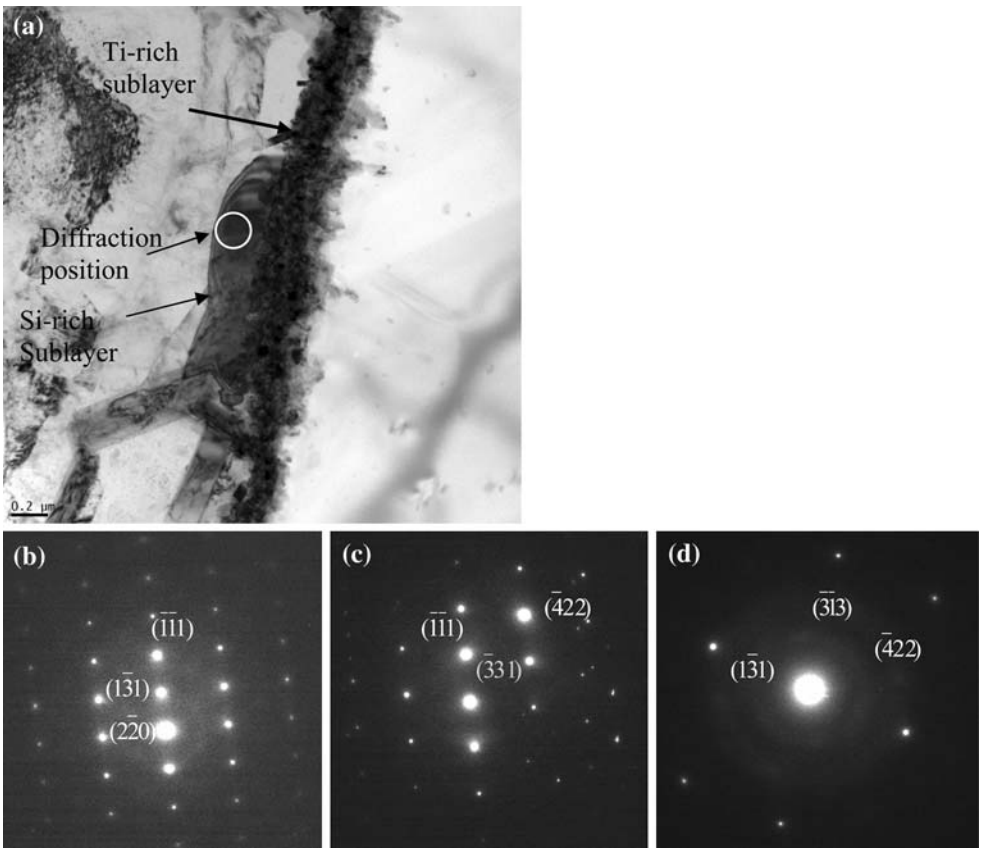

Fig. 12 Si-rich sublayer observation (Si) and its identification: (**a**) a TEM bright-field image showing the Si-rich sublayer close to the Ti-rich sublayer and a diffraction position; (**b**–**d**) are the corresponding selected area electron diffraction patterns from Si at the respective zone axes [112], [213], and [435]

In location B, three sublayers have also been detected in the barrier layer (Figs. 8 and 9b). The first sublayer close to the B_4C particles is the Al-rich layer composed of Al_3BC crystals, which is identical to that in location A. The second sublayer is the Ti-rich layer composed of fine TiB_2 crystals. However, this layer is much thinner than the layer in location A. This sublayer is followed by a layer consisting of some coarse stick-shaped Ti-rich particles, in which traces of Al, C, Mg, and Si were detected (Figs. 8 and 9b). The selected area diffraction patterns of the stick-shape particles indicate that the coarse particles are TiB_2 (Fig. 13). Contrary to location A, no Si crystals were detected here. Overall, the barrier layer is significantly less dense than the one in location A due to the coarse TiB_2 particles. Table 3 gives an overview of the structure, chemical composition and compounds in the barrier layer.

Based on the above observations, it is believed that, as the B_4C particles are injected into the liquid, they first react with liquid aluminum to form Al_3BC compounds. With a reasonable level of Ti in the melt, Ti will also react with B to form TiB_2, as Ti has a higher affinity with B than aluminum does [2]. As the reaction continues, the TiB_2 layer, in the form of fine crystals, encloses the first tiny Al-rich layer and extends around all surfaces of the B_4C particles. This TiB_2 layer at the interface acts as a rate limiting barrier to decrease the decomposition of B_4C in the liquid aluminum. In the Al–Si–B_4C composite, it is certain that Si promotes the formation of a dense TiB_2 barrier layer, thus enhancing the stability of the B_4C particles. This is probably due to the contribution of constitutional undercooling from the silicon concentration in the region of Al–Si eutectics. In other words, in the region where there is no silicon concentration, the TiB_2 crystals, whose growing directions are similar to the heat-flow, will grow without restriction and become much coarser.

Conclusions

(1) The B_4C particle distribution in the cross-section of the cast part is not uniform. More particles concentrate in the center and fewer particles locate in the wall regions. However, statistical analysis shows that the average particle fraction in different sections is more or less uniform.

(2) Some segregation bands that contain fewer particles than the average particle fraction are observed in the microstructure of the die cast part. The mechanisms of the particle migration during solidification are discussed.

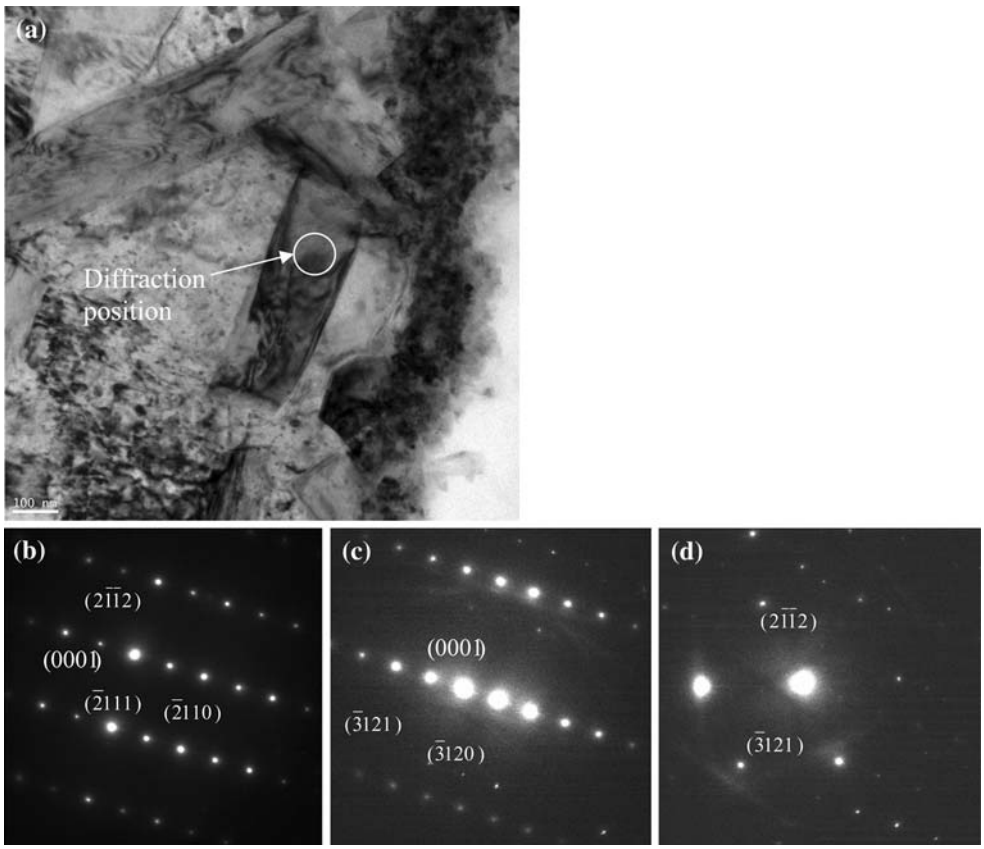

Fig. 13 Coarse stick-shaped particles and their identification: (**a**) a TEM bright-field image showing the stick-shaped particles and a diffraction position; (**b–d**) are the corresponding selected area electron diffraction patterns from TiB_2 at the respective zone axes [0$\bar{1}$10], [1$\bar{5}$40], and [2$\bar{1}\bar{3}$11$\bar{3}$]

Table 3 Overview of the structure, composition, and compounds of the barrier layer

Barrier layer	Location A			Location B		
Sublayers	Al-rich	Ti-rich	Si-rich	Al-rich	Ti-rich	Ti-rich stick-shaped particles
Composition	Al, B, C (traces of Mg)	Ti, B (traces of Al, C, Mg, Si)	Si (traces of Mg, Al)	Al, B, C (traces of Mg)	Ti, B (traces of Al, C, Mg, Si)	Ti, B (traces of Al, C, Mg, Si)
Compounds	Al_3BC	TiB_2	Si particles	Al_3BC	TiB_2	TiB_2 coarse particles

(3) In the interface between B_4C particles and aluminum, a barrier layer less than 1 μm thick was detected. Its structure, chemical composition and compounds are reported in detail. It is found that the barrier layer consists of three sublayers, i.e., Al-rich (Al_3BC), Ti-rich (TiB_2), and Si eutectic or stick-shaped TiB_2.

(4) The TiB_2 sublayer limits the decomposition of B_4C particles in the aluminum matrix. Si in the composite promotes the formation of a dense Ti-rich sublayer that improves the stability of B_4C.

Acknowledgements The authors would like to acknowledge the financial support of Natural Sciences and Engineering Research Council of Canada (NSERC), Alcan Inc., Arvida Research and Development Centre (ARDC) and Centre Québécois de Recherche et de Développment de l'Aluminium (CQRDA). They would like to thank the Aluminum Technology Center (CTA) for the permission to use its high pressure die casting machine and die mould. They are also grateful to Dr. S. Nafisi, M. Bouchard, and G. Lemire of UQAC, P. Plamondon and J.-P. Masse of École Polytechnique de Montréal, and Dr. M. Choquette of Université Laval for their assistance in the microstructure examination.

References

1. Chen X-G (2006) In: Grupta N, Hunt WH (eds) Proceedings of solidification processing of metal matrix composites, TMS 2006, San Antonio, USA, March 2006, p 343

2. Chen X-G (2005) In: Schlesinger ME (ed) EPD Congress 2005. TMS 2005, p 101
3. Zhang Z, Chen X-G, Charette A (2006) In: Grupta N, Hunt WH (eds) Proceedings of solidification processing of metal matrix composites, TMS 2006, San Antonio, USA, March 2006, p 173
4. Kennedy AR (2002) J Mater Sci 37:317. DOI: 10.1023/A:1013600328599
5. Lloyd DJ (1997) In: Mallick PK (ed) Composites engineering handbook. Marcel Dekker, Inc., p 631
6. Viala JC, Bouix J, Gonzalez G, Esnouf C (1997) J Mater Sci 32:4559. DOI: 10.1023/A:1018625402103
7. Pyzik AJ, Beaman DR (1995) J Am Ceram Soc 78:305
8. Shorowordi KM, Laoui T, Haseeb ASMA, Celis JP, Froyen L (2003) J Mater Process Technol 142:738
9. Zhang Z, Chen X-G, Charette A, Ghomashchi R (2005) In: Martin J-P (ed) Proceedings of 44th annual conference of metallurgist of CIM, Calgary, Canada, August 2005, p 447
10. Laukli H, Lohne O, Arnberg L (2005) In: Tiryakioglu M, Crepeau PN (eds) Proceedings of TMS 2005 – shape casting – The John Campbell symposium, San Francisco, USA, February 2005, p 263
11. Sannes S, Westengen H (1998) In: Mordike BL, Kainer KU (eds) Proceedings of magnesium alloys and their application, Wolfsburg, Germany, April 1998, p 223
12. Laukli H, Gourlay C, Dahle A, Lohne O (2005) Mater Sci Eng A 413–414:92
13. Gourlay CM, Laukli HI, Dahle AK (2004) Metall Mater Trans A 35A:2881
14. Laukli H, Lohne O, Armberg L (2005) In: Tiryakioglu M, Crepeau PN (eds) Proceedings of shape casting – The John Campbell symposium, San Francisco, USA, February 2005, p 263
15. Dahle AK, St John DH (1999) Acta Mater 47:31
16. Rohatgi PK, Asthana R, Yarandi F (1989) In: Rohatgi P (ed) Proceedings of solidification of metal matrix composites, Indianapolis, pp 51–75
17. Lin CB, Wu CL, Chiang CH (1999) J Mater Sci 34:2229. DOI: 10.1023/A:1004557103809
18. Lin CB, Ma CL, Chung YW (1998) J Mater Process Technol 48:236
19. Lee TW, Lee CH (2000) J Mater Sci 35:4261. DOI: 10.1023/A:1004819931889
20. Ares A, Caram R, Schvezov C (2006) In: Gupta N, Hunt WH (eds) Proceedings of TMS 2006 – solidification process of metal matrix composites (Rohatgi Honorary Symposium), San Antonio, USA, March 2006, p 183
21. Ferguson J, Kemblowski Z (1991) Applied fluid rheology. Elsevier Applied science, London, p 199
22. Powder Diffraction File No. 50-1470, and 35-0741 (2003) International Center for Diffraction Data, Newtown Square, PA, USA
23. Powder Diffraction File No. 05-0565 (2003) International Center for Diffraction Data, Newtown Square, PA, USA